Thermodynamic Linkage in the GrpE Nucleotide Exchange Factor, a Molecular Thermosensor†

Amy D. Gelinas, Joseph Toth, Kelley A. Bethoney, Knut Langsetmo, Walter F. Stafford, and Celia J. Harrison*

Boston Biomedical Research Institute, 64 Grove Street, Watertown, Massachusetts 02472

Received March 17, 2003; Revised Manuscript Received June 10, 2003

ABSTRACT: GrpE is the nucleotide exchange factor for the *Escherichia coli* molecular chaperone DnaK, the bacterial homologue of Hsp70. In the temperature range of the bacterial heat shock response, the long helices of GrpE undergo a helix-to-coil transition, and GrpE exhibits non-Arrhenius behavior with respect to its nucleotide exchange function. It is hypothesized that GrpE acts as a thermosensor and that unwinding of the long helices of *E. coli* GrpE reduces its activity as a nucleotide exchange factor. In turn, it was proposed that temperature-dependent down-regulation of the activity of GrpE may increase the time in which DnaK binds its substrates at higher temperatures. A combination of thermodynamic and hydrodynamic techniques, in concert with the luciferase refolding assay, were used to characterize a molecular mechanism in which the long helices of GrpE are thermodynamically linked with the β-domains via an intramolecular contact between Phe86 and Arg183. These "thermosensing" long helices were found to be necessary for full activity as a nucleotide exchange factor in the luciferase refolding assay. Point mutations in the β-domains and in the long helices of GrpE destabilized the β-domains. Engineered disulfide bonds in the long helices alternately stabilized the long helices and the four-helix bundle. This allowed the previously reported 75 °C thermal transition seen in the excess heat capacity function as monitored by differential scanning calorimetry to be further characterized. The observed thermal transition represents the unfolding of the four-helix bundle and the β-domains. The thermal transitions for these two domains are superimposed but are not thermodynamically linked.

The adenosine triphosphate hydrolyzing activity of the bacterial molecular chaperone DnaK (Hsp70) is stimulated by the cochaperones DnaJ and GrpE. In turn, these two molecules appear to control the duration that nascent polypeptides, portions of macromolecular assemblies, and other unfolded hydrophobic polypeptide substrates are sequestered from the crowded macromolecular environment by the DnaK substrate-binding domain. The DnaK molecular chaperone cycle operates constitutively and under cell stress conditions induced by exposure to heat, ethanol, heavy metals, and unnatural amino acids (reviewed in refs *1*−*3*). DnaJ stimulates the intrinsically weak ATP-hydrolyzing activity of DnaK. GrpE interacts with the ADP-bound conformation of DnaK and greatly accelerates nucleotide exchange by forming a stable complex with DnaK in an open conformation that is inconsistent with high-affinity ADP binding. ATP then rapidly displaces GrpE from DnaK. Concomitant with ATP binding, protein substrates are released from the DnaK substrate binding domain; after ATP hydrolysis, the ADP-bound form of DnaK has high affinity for those protein molecules that inappropriately expose hydrophobic stretches and are thus prone to irreversible protein aggregation.

The cocrystal of GrpE with the ATPase domain of DnaK shows that GrpE is an asymmetric dimer that pries open the nucleotide binding cleft of DnaK (*4*). GrpE thus accelerates ADP release 5000-fold (*5*). GrpE is a homodimer at the level of the primary structure, but the quaternary structure of GrpE is heterodimeric in the cocrystal with $DnaK_{ATPase}$ (Figure 1). Despite the asymmetric appearance of the GrpE heterodimer, the two halves of the "headpiece" (half of the four-helix bundle and one β-domain) are largely superimposable. This suggests that the role of asymmetry in the GrpE dimer may be to promote the stable interdomain interaction by Phe86 in the long helices and Arg183 in the β-domain in the GrpE monomer that is proximal to DnaK. It is hypothesized that the intramolecular contacts between Phe86 and Arg183 are important for the observed temperature dependence of the nucleotide exchange activity of GrpE.

Thermodynamic analysis of GrpE using DSC[1] revealed two thermal transitions in the excess heat capacity function. By using a combination of DSC, circular dichroism spectroscopy, and sedimentation velocity analytical ultracentrifugation, the long helices of GrpE were assigned to the first thermal transition (T_m ∼50 °C) in the excess heat capacity function, and the four-helix bundle was assigned to the second thermal transition (T_m ∼75 °C) (*6*). To assess the possible thermodynamic linkage between the long helices and the β-domains, which contribute most, but not all, of the important intermolecular contacts to DnaK (Gelinas et al., manuscript in preparation), it is necessary to demon-

† This work was supported by NIH Grant R01GM58256 to C.J.H.
* Corresponding author. E-mail: harrison@bbri.org.

[1] Abbreviations: AUC, analytical ultracentrifugation; DSC, differential scanning calorimetry; wt, wild type; T_m, midpoint temperature of thermal transition; CD, circular dichroism.

10.1021/bi034416b CCC: $25.00
Published on Web 07/11/2003

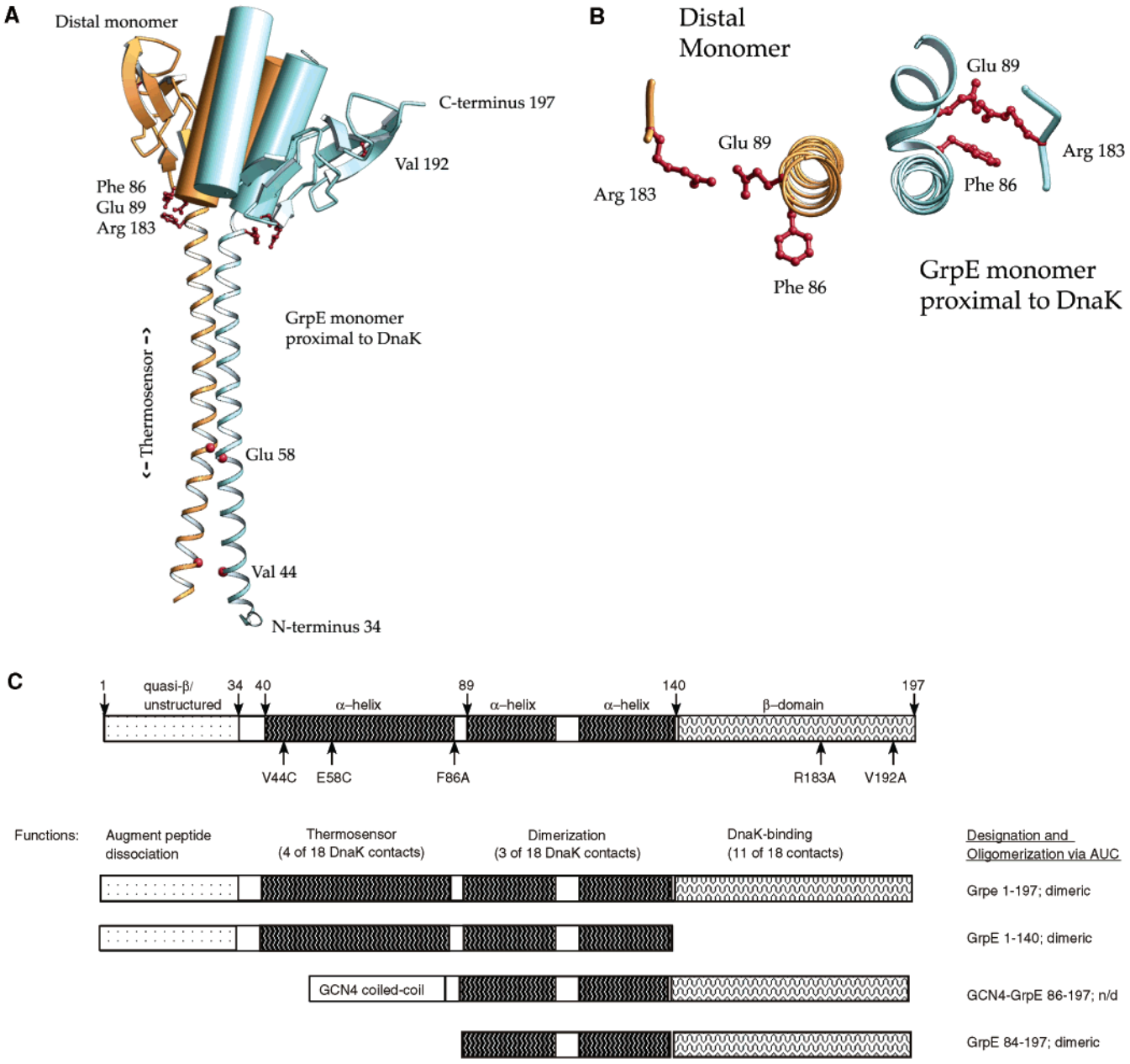

FIGURE 1: (A) A ribbon and cylinder drawing of the nucleotide exchange factor GrpE. The thermosensing long helices of GrpE (residues 40−88) are drawn as thin ribbons to represent their role as temperature sensors capable of undergoing reversible melting at temperatures relevant to heat shock. The four-helix bundle (residues 89−139) is drawn as cylinders to represent how the structural domain acts as a stable platform for the association of the long helices. The compact β-domains (residues 140−197) are drawn as ribbons. The structure is shown as the asymmetric dimer as it appears in the crystal structure of the complex with the DnaK ATPase domain (PDB 1DKG) Positions 44 and 58, which were mutated to cysteine in this study, are indicated by red balls. In addition, the side chains Phe86, Glu89, Arg183, and Val192 are drawn in red ball-and-stick representation. (B) A close-up of the intramolecular contacts seen in the asymmetric dimer. On the left is Phe86, Arg183, and Glu89 of the monomer that does not contact DnaK; on the right is Phe86, Glu 89, and Arg183 in the GrpE monomer that contacts DnaK. DnaK is not shown for clarity. These images were composed with Molscript (*20*) and converted to POVRAY (www.povray.org) format (D. Jeruzalmi, unpublished) with which they were rendered. (C) Domain organization of *E. coli* GrpE with secondary structure and point mutants studied in this paper indicated.

strate that the thermal transition of the β-domain is also part of the 75 °C thermal transition and to determine the enthalpic contribution of the β-domains to that thermal transition. This was accomplished by studying specific point mutants of the GrpE β-domains and by specifically enhancing the stability of the long helices and the four-helix bundle.

Escherichia coli GrpE was recently found to have reduced activity as a nucleotide exchange factor at higher temperatures in assays measuring the following: (1) the rate of release of a fluorescently labeled ADP analogue from DnaK, (2) the rate of release of a fluorescently labeled peptide from the substrate binding domain, and (3) the rate of change in the intrinsic fluoresence of Trp102, which is sensitive to the nucleotide state of DnaK but not to GrpE binding (*7*). This reduced activity at higher temperatures (above 40 °C and relevant to *E. coli* heat shock) followed a non-Arrhenius trend. That is, a nonlinear dependence of rate versus the inverse of temperature was observed. Non-Arrhenius behavior can be due to a temperature-dependent conformational change, either gradual or sharp, of a component of a reaction

(*8*). In the case of GrpE and DnaK, the GrpE-dependent change in the rate of reaction, which is inferred to be GrpE-dependent nucleotide exchange, does not appear to be a distinct step function. Instead, the Arrhenius plots of the three assays in Grimshaw et al. (*7*) are smooth curves, consistent with GrpE undergoing a gradual phase transition, which is a function of the long helices (*9*). The further thermodynamic characterizations of GrpE presented here were carried out to test if the hypothesis that the temperature-dependent reduction in nucleotide release is due to the unwinding of the long helices, which occurs over the same temperature range (*6*, *9*), rather than due to the melting of the β-domains as has been indicated by the studies of *Thermus thermophilus* GrpE, which participates in a molecular chaperone cycle that is somewhat different from the *E. coli* molecular chaperone cycle in its oligomeric organization (*10*−*12*). To that end, the role of the long helices in nucleotide exchange and the role of the thermodynamic linkage between the long helices and the β-domains *in E. coli* GrpE were investigated using the luciferase refolding assay, differential scanning calorimetry, circular dichroism spectroscopy, and sedimentation velocity analytical ultracentrifugation.

MATERIALS AND METHODS

Construction of Mutants. Wild-type GrpE had been previously cloned into pET-15b; the mutations were introduced into this construct by QuikChange mutagenesis (Stratagene). The GCN4-GrpE(F86−197) was constructed by sequential PCR. Full-length DnaK was amplified from a clone, to introduce a 5′ *Nde*I site and a 3′ *Bam*HI site, suitable for cloning into pET-15b. Full-length DnaJ was amplified from a previous clone, to introduce a 5′ *Nde*I site and a 3′ *Bam*HI site, suitable for cloning into pET-15b.

Purification. Wild-type *E. coli* GrpE, GrpE mutants, full-length DnaK, and DnaJ were overexpressed in *E. coli* BL21(DE3) cells. All of the constructs used in this study initially possessed a thrombin-cleavable N-terminal hexahistadine tag, conferred by the pET-15b plasmid, which was subsequently removed by proteolysis. Wild-type GrpE and GrpE mutant proteins were purified as previously described (*6*). GrpE proteins were then subjected to proteolytic digestion with thrombin (Haemolytics) at a 1:1000 w/w ratio of thrombin to GrpE. Digestion was followed by further purification using anion-exchange chromatography with Source Q media (Amersham Pharmacia) at a pH of 8.0. Purified, digested GrpE was dialyzed against 10 mM potassium phosphate buffer, pH 6.8, and stored at −80 °C. DnaK was purified immediately after expression using Ni^{2+}-NTA affinity media (Qiagen). DnaK was further purified on an anion-exchange column using Macroprep High-Q media (Bio-Rad) at 25 °C and at pH 8.0. Purified DnaK was dialyzed against 25 mM Tris, pH 8.0, and 25 mM NaCl. DnaJ was purified using Ni^{2+}-NTA chromatography (Qiagen) at 4 °C in the presence of 400 mM urea. Following purification, DnaJ was dialyzed against 25 mM Mopso, pH 6.8, 25 mM NaCl, and 0.01% Brij-35. Following dialysis, both proteins were concentrated using an Amicon ultrafiltration device with PM-10 membranes (Millipore). DnaK was sterile filtered and stored at 4 °C for immediate use. DnaJ was stored at −80 °C or sterile filtered and stored at 4 °C for immediate use. Concentrations of GrpE were determined by the synthetic boundary method in the analytical ultracentrifuge, using interference optics and a mass extinction coefficient of 3.29 fringes per mg mL^{-1}. DnaK and DnaJ concentrations were determined by UV spectrophotometry.

Differential Scanning Calorimetry. GrpE proteins were exhaustively dialyzed versus 10 mM potassium phosphate buffer, pH 6.8, prior to differential scanning calorimetry experiments. The excess heat capacity data from the GrpE proteins were collected with a VP-DSC (MicroCal) over the range of 10−120 °C with a scan rate of 1.5 °C min^{-1}. All DSC experiments reported in this study showed thermal reversibility, which was confirmed by repeat DSC scans and CD spectroscopy. As was reported previously (*6*), GrpE(84−197) unfolds irreversibly when monitored by DSC and CD spectroscopy, and so the thermal properties of this protein fragment are not discussed.

DSC data were fit using Origin 7 (MicroCal Inc., Northampton, MA). Briefly, heat capacity data for a buffer versus buffer reference were subtracted from protein versus buffer data, and units were converted to kcal mol^{-1} of protein. Pre- and posttransition baselines were taken from the linear portion of the scans before and after any observed transitions, respectively. A progress baseline was calculated through the transitions, and the baseline was then subtracted from the data. The data were then fitted using the independent non-two-state transtions function in Origin 7:

$$C_p(T) = \frac{K_A(T)\Delta H^*_{mA}\Delta H_{mA}}{[1 + K_A(T)]^2 RT^2} + ...$$

and

$$K_A(T) = \exp\left[\frac{-\Delta H^*_{mA}}{RT}\left(1 - \frac{T}{T_{mA}}\right)\right]$$

where $C_p(T)$ and $K_A(T)$ are the heat capacity and equilibrium constant as a function of temperature, R is the gas constant, and T_{mA}, ΔH_{mA}, and ΔH^*_{mA} are the temperature at the midpoint of the transition, the calorimetric enthalpy, and the van't Hoff enthalpy for each transition, respectively.

Sedimentation Velocity Analytical Ultracentrifugation. GrpE proteins were exhaustively dialyzed versus 10 mM potassium phosphate buffer, pH 6.8, and 100 mM NaCl prior to 3-fold serial dilutions (with dialysis buffer) and loading into sector-shaped centerpieces for sedimentation velocity analytical ultracentrifugation. Data were collected at 20 °C at a speed of 50000 rpm using a BeckmanCoulter XL-I with interference optics. Data were analyzed with DCDT (*13*).

Circular Dichroism Spectroscopy. GrpE(E58C,1−197) was dialyzed exhaustively versus 10 mM potassium phosphate buffer, pH 6.8, prior to the CD experiment. An AVIV 62A DS circular dichroism spectrophotometer with a temperature controller was used to collect the data at 1.5° increments from 10 to 95 °C, with 30 s temperature equilibrations, followed by 30 s data averaging, using a 0.1 cm cuvette. Reversibility of folding was confirmed by rapidly reducing the temperature to 10 °C and repeating the scan. The midpoint of the thermal transition was taken from a plot of the first derivative of the CD signal versus temperature.

Luciferase Refolding Assay. Firefly luciferase was purchased from Promega and reconstituted in 25 mM Tris−

acetate, pH 7.8, 1 mM EDTA, 0.2 M ammonium sulfate, 15% glycerol, and 30% ethylene glycol. Luciferin, potassium salt, was obtained from Pharmingen, reconstituted in DI water, and aliquoted into light-blocking tubes. Both reagents were stored at −80 °C. ATP (disodium salt, trihydrate) and monobasic and dibasic sodium phosphate were purchased from Fisher Biotech. ATP was stored at −20 °C. Guanidine hydrochloride was acquired from VWR International. Bovine serum albumin and dithiothreitol, stored at −20 °C, were purchased from New England Biolabs and Sigma, respectively. Luciferase was denatured at 42 °C in the presence of 6 M guanidine hydrochloride, 10 mM sodium phosphate buffer, pH 6.5, and 5 mM dithiothreitol. During the assay, the denatured luciferase was kept at 42 °C. The assay commenced 30 min after luciferase was first placed at 42 °C. The luciferase refolding assay was performed at room temperature, following the procedure outlined in ref *12*. To initiate the luciferase refolding at room temperature, denatured luciferase was diluted 1:100 to a final concentration of 0.033 μM into the refolding reactions, which contained 1× buffer B, 2 mM ATP, 5 mM dithiothreitol, 10% glycerol, 0.05 mg/mL BSA, 10 μM DnaK, 4 μM DnaJ, and 0.63 μM GrpE. Reaction mixtures were centrifuged for 1 min at 16000 rpm. Luciferase activity was measured every 2 min for a period of 12 min by adding 10 μL of the refolding reaction to the luciferin cocktail. The cocktail consisted of 530 μM ATP, 3.3 mM dithiothreitol, 0.05 mg/mL BSA, 47 μM luciferin, and 1× luciferase buffer, which contained 100 mM Tricine, pH 7.8, and 5.35 mM $Mg(CO_3)_4{\cdot}Mg(OH)_2$. Luciferase activity was monitored using a MGM-Measurements Optocomp-P luminometer. All assays were done sequentially in triplicate and repeated on different days with independent preparations of the DnaK, DnaJ, and GrpE proteins.

RESULTS

The Long Helices of GrpE Are Necessary To Confer Wild-Type Levels of Nucleotide Exchange Activity. To understand the contributions of the long helices to the nucleotide exchange activity of GrpE, the luciferase refolding assay was used to assess the activity of (i) the headpiece of GrpE, which lacks the long helices, yet remains dimeric [GrpE(84−197)], (ii) a chimeric GrpE in which the long helices are removed and replaced with the coiled-coil domain of GCN4 [GCN4-GrpE(86−197)], (iii) GrpE that has been cross-linked via a disulfide bond, formed by the replacement of Val44 with cysteine [GrpE(V44C)], and (iv) GrpE point mutants that replace Arg183 or Arg183 and Phe86 with alanines. The luciferase refolding assay uses DnaK, DnaJ, GrpE, Mg^{2+}, and ATP to refold chemically denatured firefly luciferase. The extent of refolding is assayed by the ability of active luciferase to cause luciferin to emit light in an ATP-dependent manner.

The results presented in Figure 2 show first that the headpiece of GrpE [GrpE(84−197)], which retains all of the DnaK contacts found on the GrpE β-domain and on the proximal half of the four-helix bundle, has ∼30% of the wild-type nucleotide exchange activity and second that the GCN4-GrpE(86−197) chimeric nucleotide exchange factor is equally or less active than the headpiece [GrpE(84−197)]. This chimeric protein was produced by fusing the canonical coiled coil from the yeast transcription factor GCN4 to the

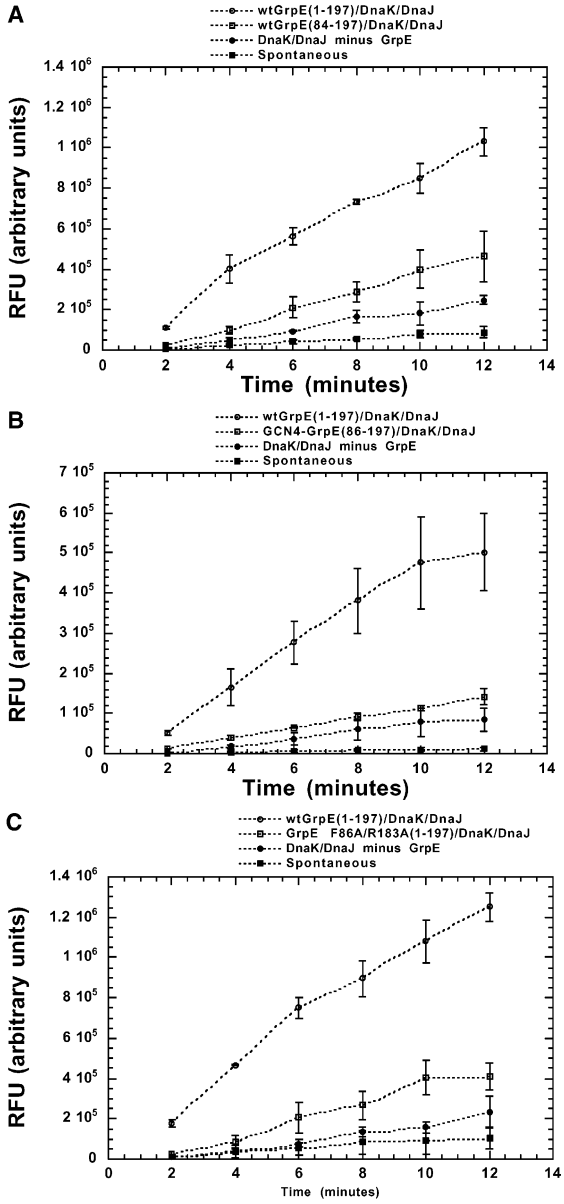

FIGURE 2: The presence of the long helices is required for wild-type levels of nucleotide exchange by GrpE in the luciferase refolding assay. (A) The headpiece of GrpE [GrpE(84−197)] is dimeric in solution (*6*) and acts weakly as a nucleotide exchange factor. Wild-type GrpE (63 nM, open circles) and GrpE(84−197) (63 nM, open squares) were added in a luciferase refolding assay (see Materials and Methods). In all panels, the unfolding reaction in the absence of GrpE is indicated with filled circles, and the spontaneous refolding of luciferase is indicated by filled squares. The *Y* axis is expressed in arbitrary light units. All assays were done in triplicate, and error bars represent the standard deviation of the result around the mean of the result. (B) The chimeric protein GCN4-GrpE(86−197), in which the canonical coiled coil from GCN4 replaces the long helices of GrpE also has diminished activity as a nucleotide exchange factor. Wild-type GrpE (63 nM, open circles) and GCN4-GrpE(86−197) (60 nM, open squares) were used in the luciferase refolding assay as in (A). (C) The double mutant, F86A/R183A, in which an intramolecular contact observed in the crystal structure (*4*) is perturbed by alanine substitutions has weak nucleotide exchange activity. Wild-type GrpE (63 nM, open circles) and GrpE(F86A/R183A) (63 nM, open squares) were added in a luciferase refolding assay as in (A). For all assays, protein concentrations for GrpE and GrpE mutants were determined by the synthetic boundary method, which is highly accurate. Not shown are data for GrpE(V44C), which were indistinguishable from wild-type GrpE, and data for GrpE(R183A), which were indistinguishable from GrpE(F86A/R183A).

headpiece of GrpE at position 86 to produce GCN4-GrpE(86−197) (*14*, *15*). This replaced the long helices of GrpE with the GCN4 leucine zipper. GCN4-GrpE(86−197) appeared well folded in the CD as demonstrated by a strong α-helical signal and exhibited reversible thermal denaturation when monitored by CD spectroscopy at 222 nm. One broad thermal transition was observed, starting around 70 °C, which is consistent with published T_ms for GCN4 (*16*) and the four-helix bundle of GrpE (data not shown). Third, the results show that GrpE(F68A/R183A) is also weakly active as a nucleotide exchange factor. Data for GrpE(R183A) are not shown and were indistinguishable from GrpE(F86A/R183A).

GrpE with a cysteine mutation introduced near the N-terminus of the long helices [GrpE(V44C,1−197)] had wild-type levels of nucleotide exchange activity when tested in the luciferase refolding assay (data not shown). The presence of a disulfide bond was demonstrated on non-reducing SDS−PAGE (data not shown).

Sedimentation Velocity Analytical Ultracentrifugation. To rule out the possibility that the dimeric GrpE(84−197) was dissociating into monomers in the luciferase refolding assay, sedimentation velocity analytical ultracentrifugation was used to investigate the concentration dependence to the sedimentation coefficient. The time−derivative plots of a dilution series of GrpE(84−197) over the concentration range of 64.9−1.9 μM show no concentration dependence to the sedimentation coefficient at 20 °C (Figure 3A). The observed sedimentation coefficient ($s_{20,b}$) of dimeric GrpE(84−197), which lacks the N-terminal hexahistidine tag, is 1.9 S, very similar to the previously reported value of 2.1 S ($s_{20,b}$) for the dimeric, hexahistidine-tagged GrpE(84−197) (*6*). This indicates that the dimer−monomer dissociation constant at 20 °C is at least 2 orders of magnitude lower (*17*) than the lowest concentration (1.9 μM) in this experiment, which is at the lower limit of detection by the interference optics.

The concentration dependence of the sedimentation coefficients of the GrpE mutants GrpE(F86A,R183A) and GrpE(V44C,1−197) were compared to wild-type GrpE(1−197). All proteins had the N-terminal hexahistidine tag removed by thrombin cleavage. The observed sedimentation coefficients ($s_{20,b}$) were 2.2 S for GrpE(F86A,R183A) (data not shown), 2.25 S for GrpE(V44C,1−197), and 2.2 S for wild-type GrpE(1−197) (Figure 3B,C). The sedimentation coefficient of 2.2 S for wild-type GrpE(1−197) was very similar to the value of 2.33 S previously reported for hexahistidine-tagged, wild-type GrpE(1−197) (*6*). None of the proteins exhibited any concentration dependence to the sedimentation coefficients in the time−derivative plots of the dilution series, indicating that none of these proteins have observable dimer-to-monomer dissociation at 20 °C. The lowest protein concentrations observed are indicated on the figure legends.

Destabilization of the β-Domains by Point Mutations. A thermodynamic linkage between the long helices and the β-domains had been suggested from previous examination of the thermal melting properties of GrpE, because deletion of the β-domains [GrpE(1−140)] destabilizes the long helices, shifting the midpoint of the thermal transition assigned to the long helices from 50 to 30 °C in both the DSC and CD (*6*). In the current study, differential scanning calorimetry was used to examine the thermal transitions of GrpE mutants in order to test the hypothesis that the intramolecular contact between Phe86 and Arg183, visible in the GrpE−$DnaK_{ATPase}$ cocrystal, is relevant to this thermodynamic linkage between the β-domains and the long helices. Several GrpE mutants proved useful for uncovering and deconvoluting the separate enthalpic contributions of the β-domains and the four-helix bundle to the 75 °C thermal transition observed in the excess heat capacity profile of wild-type GrpE. Figure 4 shows the excess heat capacity pro-

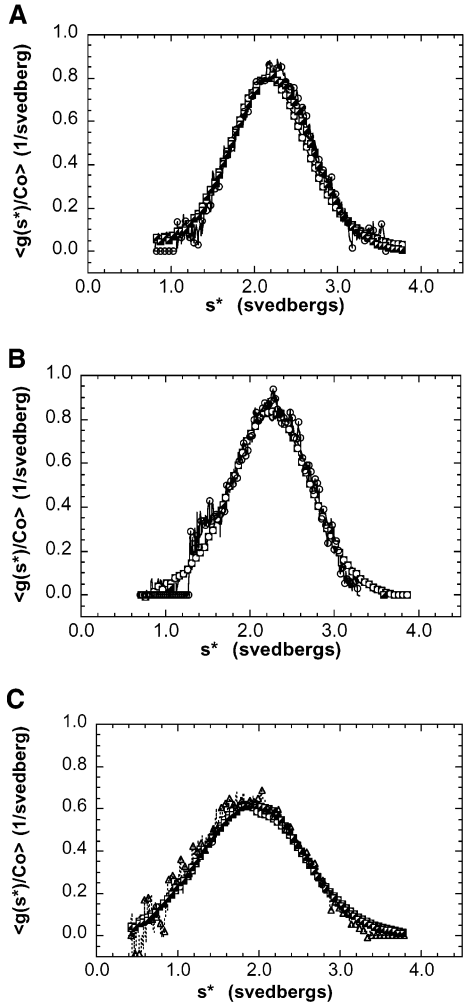

FIGURE 3: Sedimentation velocity AUC studies of mutant GrpEs reveal hydrodynamic shapes in solution and a lack of concentration dependence for the sedimentation coefficients. (A) $g(s^*)C_0^{-1}$ plots (normalized for loading concentration C_0) of a dilution series of wild-type GrpE(1−197) at three concentrations: 11.7 μM (open circle over closed square); 3.75 μM (half-filled square); 1.0 μM (open circle). (B) $g(s^*)C_0^{-1}$ plots (normalized for loading concentration C_0) of a dilution series of GrpE(V44C,1−197) at three concentrations: 9.2 μM (open circle over closed square); 2.8 μM (half-filled square); 0.72 μM (open circle). (C) $g(s^*)C_0^{-1}$ plots (normalized for loading concentration, C_0) of a dilution series of GrpE(84−197) at four concentrations; 64.9 μM (open circle over closed square); 21.7 μM (half-filled square); 6.4 μM (open circle); 1.9 μM (open triangle). All data were collected at 50000 rpm and at 20 °C. No concentration dependence to the sedimentation coefficients ($s_{20,b}$) 2.2 S [wild-type GrpE(1−197)], 2.25 S [GrpE(V44C,1−197)], and 1.9 S [GrpE(84−197)] can be seen in $g(s^*)C_0^{-1}$ plots over a range of protein concentration down to 1.0, 0.72, and 1.9 μM for wild-type GrpE(1−197), GrpE(V44C,1−197), and GrpE(84−197), respectively, suggesting that GrpE(V44C,1−197) and GrpE(84−197) remain as tightly associated as the wild-type dimeric protein and that the dissociation constants are at least 2 orders of magnitude lower than the lowest concentration of protein (*17*).

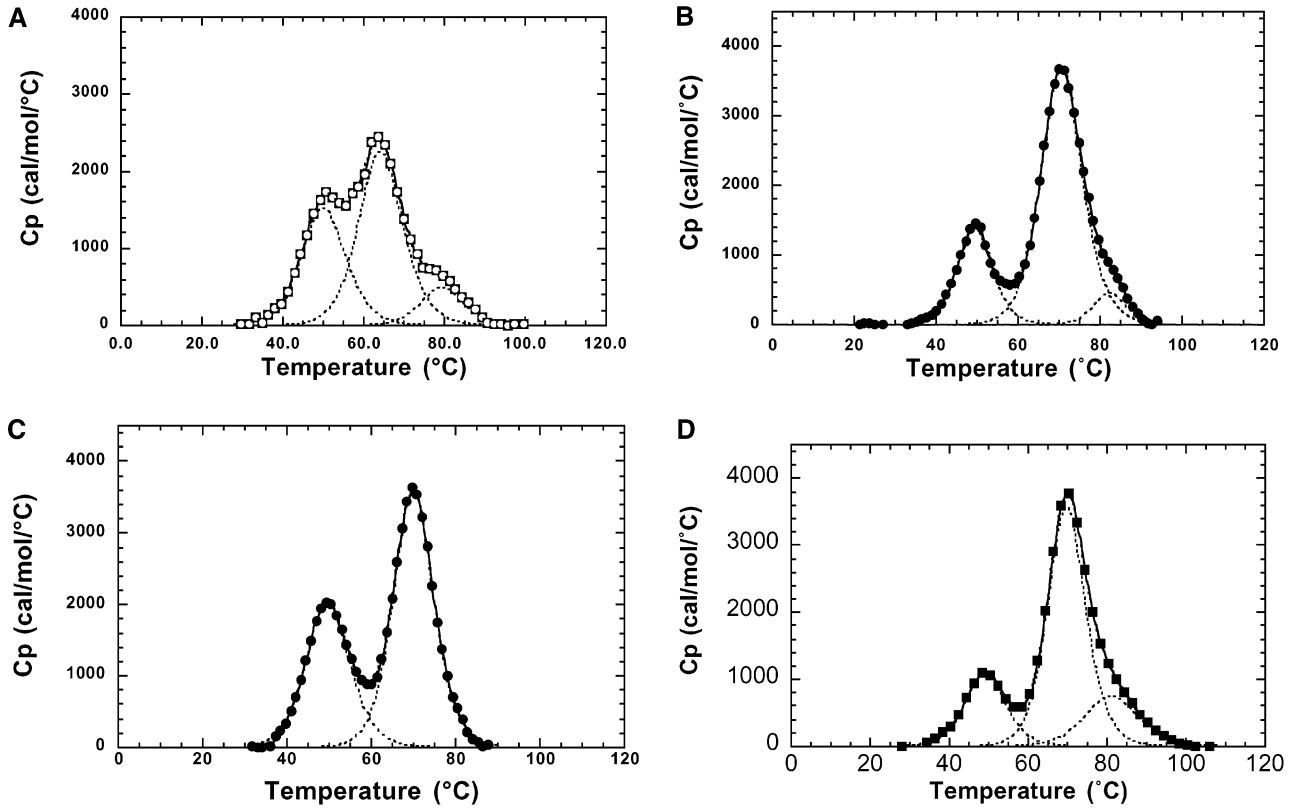

FIGURE 4: Profiles of the excess heat capacity function versus temperature for various GrpE mutants. (A) GrpE(V192A) (0.2 mg mL^{-1}, open circles over squares). The fit to the data is represented by a dashed line. (B) GrpE(F86A) (2.0 mg mL^{-1}, open circles). (C) GrpE(R183A) (2.2 mg mL^{-1}, closed circles). (D) GrpE(F86A/R183A) (1.25 mg mL^{-1}, closed squares). For comparison, the wild-type GrpE excess heat capacity profile can be seen in Figure 5A. The data were fit with Origin (MicroCal) using a non-two-state model with two or three transitions. All protein concentrations were determined by the synthetic boundary method, and additional DSC scans at lower protein concentrations (typically 0.2 mg/mL) were also collected. The concentration dependence to the T_m for the four-helix bundle was observed in GrpE(F86A) and GrpE(F86A/R183A). All constructs reported in this figure retain reversibility in their unfolding transitions (data not shown). The T_ms are tabulated in Table 1.

Table 1: Thermodynamic Parameters for GrpE Unfolding[a]

thermal transition	T_{m1} (°C)	$\Delta H_{1(cal)}$	$\Delta H_{1(vH)}$	T_{m2} (°C)	$\Delta H_{2(cal)}$	$\Delta H_{2(vH)}$	T_{m3} (°C)	$\Delta H_{3(cal)}$	$\Delta H_{3(vH)}$
wild type	50.0	19	55	75.2	46	77			
F86A	49.3	19	71	70.9	40	80	81.2	10	77
R183A	49.8	27	61	70.1	45	74			
F86A/R183A	49.9	24	52	69.8	55	67	82.9	14	54
V192A	50.1	22	57	64.3	32	63	79.6	7	70
wt,1−140	28.9	19	47	no[b]			77.9	23	56
E58C,1−197	no[c]			77.5	66	86	97.9	17	77
V44C,1−197	67.0	8	68	76.8	37	78	94.5	13	67
V44C,1−140	51.2	16	53	no[b]			91.6	19	67

[a] The midpoints of the thermal transitions are indicated, along with the calorimetric and van't Hoff enthalpies reported in kcal mol^{-1}. DSC measurements were done at 2.0 and 0.2 mg mL^{-1} for wild-type GrpE(1−197), GrpE(V192A), GrpE(V44C,1−197), GrpE(V44C,1−140), and GrpE(E58C,1−197). GrpE(F86A) was studied at 2.0 and 0.45 mg mL^{-1}. GrpE(R183A) was studied at 2.2 and 0.2 mg mL^{-1}. For GrpE(F86A/R183A), the protein concentrations were 1.25 and 0.2 mg mL^{-1}. The concentration dependence of the T_m for the four-helix bundle was observed in GrpE(F86A) and GrpE(F86A/R183A), and so the T_m is reported for the higher protein concentration. For wild-type GrpE(1−140), the highest protein concentration was 0.99 mg mL^{-1}. All constructs reported in this table retain reversibility in their unfolding transitions in the DSC [data shown for GrpE(V44C,1−197) in Figure 5B]. [b] The β-domain is not present in this construct, so the values are reported in the columns that correspond to the helical bundle. [c] The lower transition is superimposed on the second and cannot readily be deconvoluted, so the values are reported in the columns corresponding to the β-domain.

files for the single alanine point mutants GrpE(V192A), GrpE(F86A), and GrpE(R183A) and the double point mutant GrpE(F86A,R183A); T_ms and enthalpies are tabulated in Table 1. The point mutants GrpE(F86A) and GrpE(R183A) had similar decreases (∼5 °C) in the T_m of the upper thermal transition. A very slight concentration dependence (∼1.2 °C) of the thermal transition for the long helices was observed in GrpE(F86A). Previously, even this small amount of variation in the T_m of the long helices had never been observed for full-length constructs. The T_m of the long helices in a 0.45 mg mL^{-1} sample of GrpE(F86A) was a total of 2 °C lower than the T_m normally observed for this transition in wild-type GrpE (data not shown). In a 2.0 mg mL^{-1} sample of GrpE(F86A), a third transition appears reproducibly, at a T_m of 81.2 °C (Figure 4B). Presumably, this third thermal transition with its slight concentration dependence corresponds to the four-helix bundle because it so closely resembles the thermal transition of the four-helix bundle in

the C-terminally truncated GrpE(1−140) construct, which lacks the β-domains. At the lower protein concentration of 0.45 mg mL^{-1}, this third transition in GrpE(F86A) is presumably superimposed with the transition of the β-domain and is not readily deconvoluted from the baseline-subtracted excess heat capacity function. GrpE(R183A) did not reveal a third thermal transition at a protein concentration of 2.2 mg mL^{-1}, and the T_m of the long helices was slightly lower than the wild-type value (49.5 vs 50 °C).

The single point mutant GrpE(V192A) and the double mutant GrpE(F86A,R183A) also appear to have three thermal transitions, now revealing separate thermal transitions for the β-domains and the four-helix bundle. The thermal transitions are interpreted in the following order: long helices (∼50 °C), β-domains (64.3 °C for V192A, 69.8 °C for F86A, R183A), and four-helix bundle (79.6 °C for V192A, 82.9 °C for F86A,R183A). The GrpE(F86A) and GrpE(F86A, R183A) proteins demonstrated concentration dependence of the T_ms of the four-helix bundle. In the lower concentration tested of GrpE(F86A), 0.45 mg mL^{-1}, the thermal transition corresponding to the four-helix bundle is still superimposed (to the point that the two transitions cannot be deconvoluted) with that of the β-domain, despite the fact that the β-domain has been destabilized, while in the F86A/R183A mutant, the third transition corresponding to the four-helix bundle is readily discernible at 0.2 mg mL^{-1}, as well as at 1.25 mg mL^{-1} (Table 1).

Stabilization of the Long Helices by Disulfide Bonds. Experiments were designed to deliberately stabilize the long helices (*9*, *18*, *19*), to see if there would be an effect on the stability of the β-domains. It can be seen in Figure 5 that stabilizing the long helices via a disulfide bond [GrpE(V44C,1−197)] confers ∼17 °C thermal stability to the long helices and ∼19 °C thermal stability to the four-helix bundle, shifting the latter thermal transition out from under the thermal transition of the β-domain, which exhibits a very small change in T_m (∼76.8 versus 75.0 °C in wild-type GrpE). This is further evidence that the thermal transitions for the β-domains and the four-helix bundle are superimposed in wild-type GrpE. In the C-terminally truncated mutant GrpE(V44C,1−140) in which the β-domains are missing, the long helices are again destabilized by the absence of the β-domains, which is offset by the thermal stability imposed by the disulfide bond at position 44. Figure 5 also shows the excess heat capacity profiles for the equivalent wild-type constructs for comparison. Similar results were seen with the engineered disulfide bond at position 58 [GrpE(E58C,1−197)], which is about halfway along the length of the long helices. In this protein the long helices were stabilized to the point (∼77.5 °C) that the helical thermal melting transition was now close enough to the thermal transition of the β-domains that the two could not be deconvoluted in the DSC (Figure 5C). The four-helix bundle of GrpE(E58C,1−197) is now ∼97.9 °C. To confirm this result, the temperature-induced unfolding of GrpE(E58C,1−197) was followed in a CD spectrophotometer. The β-domains are spectroscopically silent in the CD, and so the observed transition with a midpoint of ∼75 °C could be reasonably assigned to the long helices (data not shown). The unfolding transition for the four-helix bundle could not be discerned in the CD as the upper temperature limit of the machine is 95 °C. There was no

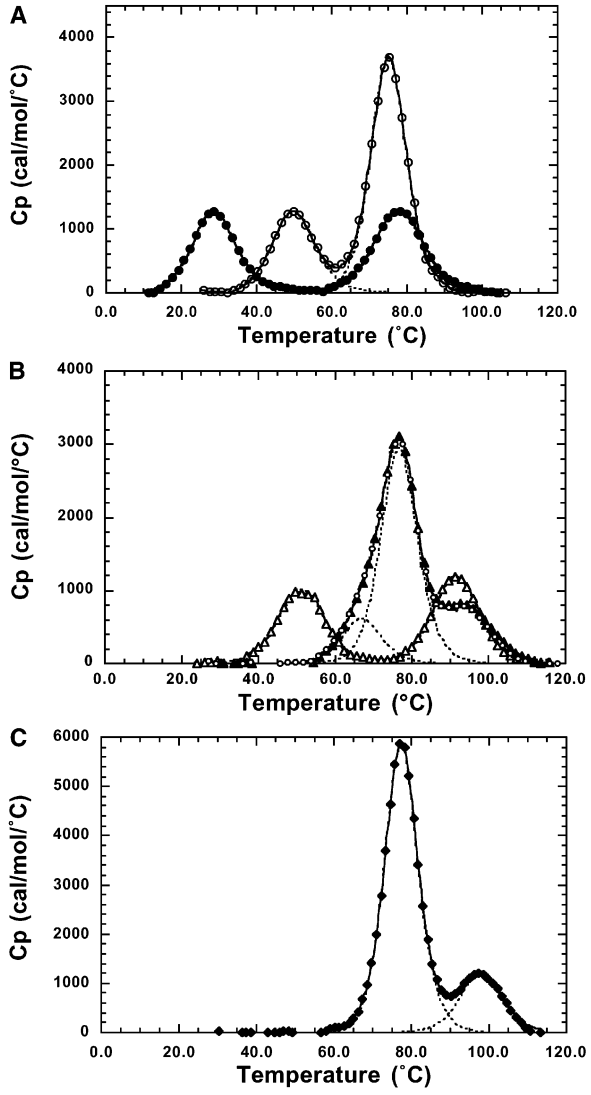

FIGURE 5: Differential scanning calorimetry was used to follow the temperature-induced unfolding transitions of wild-type GrpE, GrpE(V44C), and GrpE(E58C). In the latter two constructs, a disulfide bond was engineered by site-directed mutagenesis near the beginning and the middle of the long helices, respectively. (A) Excess heat capacity profiles versus temperature for wild-type GrpE(1−197) (2.0 mg mL^{-1}, open circles) and wild-type GrpE(1−140) (0.99 mg mL^{-1}, closed circles). The peaks in the excess heat capacity profile represent the thermal unfolding transition. The data were fit with Origin (MicroCal) using a non-two-state model with two transitions; the fits are represented by the solid and short-dashed lines for the wild-type GrpE(1−197) and wild-type GrpE(1−140) constructs, respectively. (B) Excess heat capacity profiles versus temperature for GrpE(V44C,1−197) (2.0 mg mL^{-1}, closed triangles) and GrpE(V44C,1−140) (2.0 mg mL^{-1}, open triangles) and the repeat unfolding of GrpE(V44C,1−197) (2.0 mg mL^{-1}, open circles). The data were fit with Origin (MicroCal) using a non-two-state model with two or three transitions; the fits are represented by the solid and short-dashed lines for the GrpE(V44C,1−197) and GrpE(V44C,1−140) constructs, respectively. (C) Excess heat capacity profile versus temperature for GrpE(E58C,1−197) (2.0 mg mL^{-1}, closed diamonds). The data were fit with Origin (MicroCal) using a non-two-state model with two transitions; the fit is represented by the dashed line. All protein concentrations were determined by the synthetic boundary method, and additional DSC scans at lower protein concentrations (typically 0.2 mg/mL) were also collected. No concentration dependence to the T_m was observed for any thermal transition. All constructs reported in this figure retain reversibility in their unfolding transitions [data shown for GrpE(V44C,1−197)]. The T_ms are tabulated in Table 1.

concentration dependence to any thermal transition seen in the GrpE(E58C,1−197), GrpE(V44C,1−197), and GrpE-(V44C,1−140). In Table 1 the T_ms and the enthalpies for the wild-type and disulfide-bonded constructs are tabulated.

DISCUSSION

E. coli GrpE has been called a molecular thermosensor (*6*, *9*, *12*), since the long helices unwind with increasing temperature and appear to transmit the temperature information to DnaK by reducing nucleotide exchange activity at temperatures relevant to the heat shock response. It had been previously concluded that the upper transition, in both the excess heat capacity function monitored by DSC and thermal melts monitored by CD spectroscopy, was assignable to the four-helix bundle of GrpE (*6*). Since the thermal transitions of the β-domains had not been directly investigated, it remained uncertain whether this thermal transition had enthalpic contributions from the β-domains as well. It has now been confirmed that the thermal transitions of the β-domains and the four-helix bundle examined by DSC are superimposed in wild-type GrpE, by inference from the shift in the T_m of the upper thermal transitions for the mutants GrpE(V192A), GrpE(R183A), GrpE(F86A, R183A), and GrpE(V44C) that revealed a thermal transition assignable to the four-helix bundle. The former two mutations are located within the β-domains (Figures 1 and 4) and adversely affect the thermal stability of these small domains but do not exert any thermodynamic influence on the long helices. Thermal unfolding of the β-domains can be described as a simple two-state process in which the native structure transits to an unfolded structure, with no intermediate unfolded state, a conclusion based on the calorimetric and van't Hoff enthalpies observed for this transition. The mutation V192A reduces the upper T_m by ∼10 °C; the mutation R183A reduces the T_m by ∼5 °C. The first mutation is easy to interpret: Valine 192 is well buried in what serves as a very small hydrophobic core for the β-domains. Despite the modest nature of a valine to alanine substitution, there is no doubt that a change in the packing of the small hydrophobic core would result, perturbing other residues. The arginine 183 to alanine substitution can be easily interpreted by accepting the argument that the intramolecular contacts observed in the crystal structure, both between Phe86 and Arg183 in the proximal monomer and between Arg183 and Glu89 in the distal monomer, are relevant to the thermal stability of the β-domains (Figure 1B). In support of this hypothesis that the Phe86/Arg183 intramolecular contact is part of an allosteric mechanism that informs the β-domains that the long helices have changed conformation, the mutant Grpe(F86A), which does not reside in the β-domains, but at the top of the long helices, causes a destabilization of the upper transition by ∼4 °C. It cannot be assumed a priori that in the GrpE(F86A) mutant the observed thermal destabilization is a result of destabilization of the β-domain alone and not the four-helix bundle which immediately follows the mutated position. However, in the double mutant GrpE(F86A/R183A) the thermal transition of the β-domain has been shifted sufficiently (downward by ∼6 °C to 69.8 °C) to allow the deconvolution of the thermal transition corresponding to the four-helix bundle with a T_m of 82.9 °C. There is sufficient agreement between the T_m revealed for the four-helix bundle in this GrpE(F86A/R183A) double mutant and the T_m revealed for the four-helix bundle (∼79.8 °C) in the GrpE(V192A) mutant, suggesting that the GrpE(F86A) single mutant and the GrpE(F86A/R183A) double mutant do not strongly influence the stability of the four-helix bundle. There is good agreement between the T_m of the upper transition now assigned to the four-helix bundle and the T_m seen in thermal melts followed by CD spectroscopy at 222 nm, in which the β-domains are spectroscopically silent (*6*; data not shown). Thus the Phe86/Arg183 intramolecular contact is a powerful means for communicating thermodynamic information from the long helices to the β-domains.

The third thermal transition, assigned now to the four-helix bundle, shows a slight concentration dependence for the thermal-induced dimer dissociation into unfolded monomers for constructs containing the alanine at position 86. The decrease in stability of the β-domain in the alanine point mutants F86A and F86A/R183A compared to wild-type GrpE allows this transition to be observed. The slight concentration dependence of the T_m for the four-helix bundle in these mutants suggests that perturbation of the junction between the N-terminal long helices and the four-helix bundle changes the dissociation constant of the four-helix bundle enough to observe the concentration dependence of T_m at the experimental concentrations used here (see ref *16* for an experimental demonstration of how the fraction unfolded of a dimeric molecule can vary with respect to protein concentration as a function of temperature). R183A has an altered T_m for the β-domain, but it is an insufficient change in T_m to reveal the thermal transition of the four-helix bundle, even at the high protein concentration of 2.2 mg mL^{-1}. It is likely that the four-helix bundle is melting at its native T_m, but it is impossible to address concentration dependence in the R183A mutant. The V192A mutant has a sufficiently destabilized β-domain such that the T_m of the four-helix bundle is revealed and no concentration dependence is observed, suggesting that the V192A mutant does not influence the four-helix bundle in the same way that the F86A mutation does [T_ms for the four-helix bundle transition: 79.8 °C at 2.0 mg mL^{-1} (DSC data not shown), 79.6 °C at 0.2 mg mL^{-1} (DSC data shown in Figure 5A)]. It is expected that a concentration dependence for the T_m of the four-helix bundle in wild-type GrpE and the R183A and V192A point mutants might be observed if it were possible to monitor the thermal denaturation of four-helix bundle at low enough protein concentrations.

Deletion of the β-domains [e.g., GrpE(1−140)] results in a strong destabilization of the long helices, with little or no consequence to the stability of the four-helix bundle (*6*). This suggests that the alanine perturbations of the intramolecular contact Phe86-Arg183 by either the single mutant R183A or the double mutant F86A/R183A, which do not result in destabilization of the long helices, are an incomplete model system for understanding how the β-domains reciprocally stabilize the long helices. Disulfide bonds were engineered into the long helices of GrpE to test how increasing stability of the long helices might influence the stability of the β-domains. When a disulfide bond was engineered at the beginning [GrpE(V44C,1−197)] or in the middle [GrpE-(E58C,1−197)] of the long helices, the helices were indeed thermodynamically stabilized (Figure 5). This increased

stability of the long helices also enhanced the thermal stability of the four-helix bundle, shifting the transition out from under the thermal transition of the β-domains, allowing the thermal unfolding transition of "wild-type" β-domains to be fit directly from the data. Intriguingly, the β-domains do not have a concomitant increase in stability, suggesting that they are unaffected by increases in stability of the long helices or the four-helix bundle. Thus, only decreases in stability of the long helices decrease the stability of the β-domains. This is in concurrence with the hypothesis that the thermal unfolding of the long helices of *E. coli* GrpE at temperatures relevant to bacterial heat shock could influence the β-domains and result in the decreasing rates of nucleotide exchange observed in vitro (*7*, *9*).

Several other GrpE mutants were engineered to have cysteine cross-links in the long helices to confirm that thermal stability of the β-domains is not changed by increased stability of the long helices. GrpE(V44C,1−140) and GrpE(E58C,1−197) were both examined by DSC for changes in the T_ms of the various transitions (Figure 5, Table 1). The additional data support the conclusion reached by examination of GrpE(V44C,1−197). A significant thermal stabilization of the long helices does not influence the β-domains but has a large and positive impact on the stability of the four-helix bundle. Notably, the cysteine cross-link at position V44C in the construct that lacks the β-domains shifts the lower T_m up to its wild-type level of ~50 °C, compared to ~29 °C in wild-type GrpE(1−140).

The functional significance of the various mutants examined in this study was tested using the luciferase refolding assay, which is often used to test the functionalities of DnaK, DnaJ, and GrpE in the context of the entire molecular chaperone cycle. The single and double mutants, GrpE(R183A) and GrpE(F86A,R183A), have the same reduced activity as a nucleotide exchange factor in the luciferase refolding assay as GrpEs that outright lack the long helices, such as GrpE(84−197) and the GCN4-GrpE(86−197) fusion (Figure 2). The loss of the three potential contacts made between the long helices of GrpE and DnaK (GrpE residues Arg73, Arg74, and Lys82) appears to be functionally significant by their loss in the GCN4-GrpE(86−197), and this loss is not offset by the presence of the dimeric leucine zipper. Oddly, the GrpE headpiece alone, GrpE(84−197), seems to possess slightly more activity in the luciferase refolding assay than GCN4-GrpE(86−197). Perhaps the fusion protein allows less flexibility for proper positioning of Phe86 relative to Arg183, and thereafter to DnaK, than does GrpE(84−197). Cysteine cross-linked GrpE(V44C) was fully active in the luciferase refolding assay, which suggests that the tertiary structure of the cross-linked long helices is very similar to the wild-type structure and that changes in the thermal properties of GrpE(V44C) are a result of the cross-link alone and not a gross structural perturbation introduced by the disulfide bond.

CONCLUSIONS

In keeping with the hypothesis that thermal destabilization of the long helices of *E. coli* GrpE at heat shock temperatures reduces the rate of nucleotide and substrate release from DnaK, it was found that the long helices and the β-domains are thermodynamically linked and that the intramolecular contact between Phe86 and Arg183 is part of this linkage. It has been shown that the second, upper thermal transition observed during GrpE unfolding in the DSC is comprised of enthalpic contributions from both the β-domains and the four-helix bundle, but no significant thermodynamic linkage between these two domains was observed. It had been previously observed that destabilization of the long helices by deletion of the β-domains did not affect the thermal stability of the four-helix bundle. In this study, it was shown that stabilization of the long helices by disulfide bonding reciprocally stabilizes the four-helix bundle but not the β-domains. It is as if there is a one-way flow of information, destabilization of the long helices destabilizes the β-domains, but imparting thermal stability to the long helices does not influence the β-domains. Finally, it was shown that the long helices of GrpE are required to confer full activity of GrpE as a nucleotide exchange factor, using the luciferase refolding assay. There are two possible and nonexclusive reasons for this: (1) The three residues of GrpE that are located along the long helices (Arg73, Arg74, and Lys82) that contact DnaK are required for efficient nucleotide exchange. This conclusion would be supported in part by results of Craig and co-workers, which revealed that the alanine substitution of the equivalent of Lys82 in the yeast mitochondrial GrpE, Mge1p, had reduced activity in the luciferase refolding assay. (2) The long helices are necessary to promote the stabilizing intramolecular contact between Phe86 and Arg183.

ACKNOWLEDGMENT

The authors thank Malgorzata Boczkowska, Tyler Cutforth, Zenon Grabarek, and Nick Rhind for critical reading of the manuscript. For help and advice with the luciferase refolding assay, the authors thank Manajit Hartl, Phillip Christen, and members of the Christen laboratory. The authors also thank David Jeruzalmi for advice and assistance with figure making.

REFERENCES

1. Hartl, F. U., and Hayer-Hartl, M. (2002) *Science 295*, 1852−1858.
2. Lund, P. (2001) *Adv. Microbiol. Physiol. 44*, 93−140.
3. Bukau, B., and Horwich, A. L. (1998) *Cell 92*, 351−366.
4. Harrison, C. J., Hayer-Hartl, M., Di Liberto, M., Hartl, F., and Kuriyan, J. (1997) *Science 276*, 431−435.
5. Packschies, L., Theyssen, H., Buchberger, A., Bukau, B., Goody, R. S., and Reinstein, J. (1997) *Biochemistry 36*, 3417−3422.
6. Gelinas, A. D., Langsetmo, K., Toth, J., Bethoney, K. A., Stafford, W. F., and Harrison, C. J. (2002) *J. Mol. Biol. 323*, 131−142.
7. Grimshaw, J. P., Jelesarov, I., Schonfeld, H. J., and Christen, P. (2001) *J. Biol. Chem. 276*, 6098−6104.
8. Gutfreund, H. (1998) *Kinetics for the Life Sciences*, Cambridge University Press, Cambridge, U.K.
9. Grimshaw, J. P., Jelesarov, I., Siegenthaler, R. K., and Christen, P. (2003) *J. Biol. Chem. 278*, 19048−19053.
10. Schlee, S., and Reinstein, J. (2002) *Cell. Mol. Life Sci. 59*, 1598−1606.
11. Groemping, Y., Klostermeier, D., Herrmann, C., Veit, T., Seidel, R., and Reinstein, J. (2001) *J. Mol. Biol. 305*, 1173−1183.
12. Groemping, Y., and Reinstein, J. (2001) *J. Mol. Biol. 314*, 167−178.
13. Stafford, W. F. (1992) *Anal. Biochem. 203*, 295−301.
14. Weissenhorn, W., Calder, L. J., Dessen, A., Laue, T., Skehel, J. J., and Wiley, D. C. (1997) *Proc. Natl. Acad. Sci. U.S.A. 94*, 6065−6069.

15. Drees, B. L., Grotkopp, E. K., and Nelson, H. C. M. (1997) *J. Mol. Biol. 273*, 61−74.
16. Thompson, K. S., Vinson, C. R., and Freire, E. (1993) *Biochemistry 32*, 5491−5496.
17. Stafford, W. F. (1994) in *Modern Analytical Ultracentrifugation: Acquisition and Interpretation of Data for Biological and Synthetic Polymer Systems* (Schuster, T. M., and Laue, T. M., Eds.) pp 119−137, Birkhäuser, Boston, MA.
18. Matsumura, M., Becktel, W. J., Levitt, M., and Matthews, B. W. (1989) *Proc. Natl. Acad. Sci. U.S.A. 86*, 6562−6566.
19. Filiminov, V. V., and Rogov, V. V. (1996) *J. Mol. Biol. 255*, 767−777.
20. Kraulis, P. (1991) *J. Appl. Crystallogr. 24*, 946−950.

BI034416B